Nanoscale

Cite this: *Nanoscale*, 2012, **4**, 1509

www.rsc.org/nanoscale

PAPER

$ZnO–ZnGa_2O_4$ core–shell nanowire array for stable photoelectrochemical water splitting†

Miao Zhong,* Yanbo Li, Ichiro Yamada and Jean-Jacques Delaunay*

Received 6th October 2011, Accepted 23rd November 2011
DOI: 10.1039/c2nr11451h

A dense array of vertically aligned $ZnO–ZnGa_2O_4$ core–shell nanowires was synthesized on a large scale on an *a*-plane sapphire substrate by a simple two-step chemical vapor deposition method. The ZnO cores and $ZnGa_2O_4$ shells of the nanowires are of single crystal quality and have aligned crystallographic orientations as evidenced from XRD and TEM analyses. Mott–Schottky analysis and voltage onset from the photocurrent–voltage curve confirm an n-type semiconductor property, a flat-band potential of −0.4 V (*versus* NHE) and a carrier density of 7×10^{18} cm^{-3} for the $ZnO–ZnGa_2O_4$ core–shell nanowires. A stable and large photocurrent of 1.2 mA cm^{-2} was obtained with the $ZnO–ZnGa_2O_4$ core–shell nanowire array when used as a photoanode at an applied bias of +0.7 V (*versus* Ag/AgCl) under a 300 W xenon lamp illumination. Moreover, a low dark current of $<10^{-4}$ mA cm^{-2} was obtained at an applied bias of +0.7 V (*versus* Ag/AgCl) without light illumination for the $ZnO–ZnGa_2O_4$ nanowire array. These results suggest that the dense array of $ZnO–ZnGa_2O_4$ core–shell nanowires provides enhanced electronic properties and stable anti-photocorrosion ability and, therefore, is promising as a photoanode in photoelectrochemical water splitting.

Introduction

Semiconductor–photocatalyst core–shell nanowire arrays are regarded as an attractive class of nanostructured photoanodes for photoelectrochemical hydrogen generation. Besides the morphology-induced advantages of a large surface area, a short carrier diffusion length and a low reflectivity,[1,2] the composite core–shell heterostructure is expected to offer new functionalities and compensate for individual shortcomings so as to further satisfy the thermodynamical and chemical requirements of an efficient and stable photoanode for photoelectrochemical water splitting.[3] For example, the semiconductor core increases the light absorption and electrical conductivity, the photocatalyst shell improves the surface photoreaction and anti-photocorrosion ability, and the composite heterojunction enhances the carrier lifetime. However, the search of a suitable semiconductor and photocatalyst that realize this functional core–shell nanowire structure with single crystal quality remains a major issue.

ZnO, due to its direct band gap, low cost and ease in fabrication of various single crystal nanostructures, has been widely studied.[4,5] In addition, ZnO has a similar band gap and band edge positions to those of TiO_2,[6] but an enhanced conductivity than TiO_2, leading to its potential application as a photoanode in photoelectrochemical water splitting. However, the chemical stability of ZnO in electrolyte solution is so poor that it easily dissolves into the electrolyte solution under UV light illumination. To address this limitation, surface coating of ZnO nanowires by photo-catalytic and anti-corrosive shell layers is being investigated.

In this report, a dense array of vertically aligned and single-crystal $ZnO–ZnGa_2O_4$ core–shell nanowires was synthesized in large scale on an *a*-plane sapphire substrate by a simple two-step chemical vapor deposition (CVD) method. The $ZnO–ZnGa_2O_4$ core–shell nanowires are electrically connected at their bases through a layer of the same material. This structure is ideal for a direct integration as a photoanode in the photoelectrochemical water splitting applications. The electronic property and photocurrent performance of the $ZnO–ZnGa_2O_4$ core–shell nanowires were investigated in detail. Mott–Schottky analysis and photocurrent–voltage measurements were used to identify the flatband potential, carrier density and interface band bending of the $ZnO–ZnGa_2O_4$ core–shell nanowires. Compared to the ZnO nanowires, a more favorable energy band position for the oxidation of water and an increased carrier density for the electron transfer were obtained in the $ZnO–ZnGa_2O_4$ core–shell nanowire array. These properties improve the water-splitting performance of the $ZnO–ZnGa_2O_4$ core–shell nanowire array compared to the ZnO nanowire array. Photocurrent measurement with the $ZnO–ZnGa_2O_4$ core–shell nanowire array at an applied bias of +0.7 V (*versus* Ag/AgCl) gives a stable and large

School of Engineering, The University of Tokyo, 7-3-1 Hongo, Bunkyo-ku, Tokyo, 113-8656, Japan. E-mail: jean@mech.t.u-tokyo.ac.jp; miaozhong@lelab.t.u-tokyo.ac.jp

† This article was submitted as part of a collection highlighting papers on the 'Recent Advances in Semiconductor Nanowires Research' from ICMAT 2011.

photocurrent of 1.2 mA cm^{-2} under a 300 W xenon lamp illumination. Moreover, a very low current of $<10^{-4}$ mA cm^{-2} was obtained at +0.7 V bias (*versus* Ag/AgCl) in the dark conditions. The fabricated dense array of ZnO–$ZnGa_2O_4$ core–shell nanowires therefore is promising as a photoanode material in photoelectrochemical water splitting.

Experimental method

A dense array of ZnO–$ZnGa_2O_4$ core–shell nanowires was synthesized by a two-step CVD method. First, a dense array of ZnO nanowires was grown on an *a*-plane sapphire substrate with an Au-catalyzed CVD process. In this process, an Au-coated *a*-plane sapphire substrate was placed at the center of a vacuum furnace tube and precursors of ZnO powder and graphite powder (2 : 1 in weight) were placed at 1 cm upstream position of the sapphire substrate in the furnace tube. The furnace was operated at 1000 °C for 30 minutes with oxygen and argon gases (5 : 1 in volume ratio) flowing through the tube at a working pressure of 50 mbar. During this process, a dense array of ZnO nanowires was synthesized on the surface of the Au-coated *a*-plane sapphire. The prepared dense array of ZnO nanowires was then used as a template substrate in the second CVD process to support an epitaxial growth of the $ZnGa_2O_4$ shells on the ZnO nanowires. The ZnO nanowire array substrate was placed at a temperature position corresponding to 900 °C in the furnace tube and mixed powder of Ga_2O_3, ZnO and graphite were placed at 11 cm upstream position of the substrate. The temperature of the precursor zone was set to 1180 °C. Argon and oxygen (10 : 1 in volume ratio) were used as carrier gases at a working pressure of 50 mbar. After the second growth step, a dense array of ZnO–$ZnGa_2O_4$ core–shell nanowires was obtained.

Scanning electron microscopy (SEM) images of the prepared nanowires were taken with a Hitachi S3000N. X-Ray diffraction (XRD) patterns of the prepared nanowires were obtained with a diffractometer (Miniflex II-MW, Rigaku Co. Ltd., Japan) using the Cu Kα radiation. Transmission electron microscopy (TEM) images of the prepared ZnO–$ZnGa_2O_4$ core–shell nanowires were obtained with a JEM 2010 equipment. The UV-VIS diffuse reflectance spectra of the prepared nanowires were measured with a spectrophotometer (DRS, V-560, Jasco). The electrochemical impedance measurements of the prepared nanowires were performed by a potentiostat (VersaSTAT 4, Princeton Applied Research). The photoelectrochemical water splitting experiments performed on the photoanode of prepared nanowires were carried out in a conventional Pyrex electrochemical cell equipped with a planar window. The photocurrent measurements of the fabricated photoanodes were obtained with a potentiostat (HZ-5000, Hokuto Denko; SDPS-501C, Syrinx).

Results and discussion

Characterization

Fig. 1(a) shows an SEM image of the vertically aligned ZnO nanowires on the *a*-plane sapphire substrate after the first CVD process. It is clearly seen from Fig. 1(a) that the sidewalls of the ZnO nanowires are straight and smooth. The diameter of the ZnO nanowires is uniformly distributed around 60 nm with a length of the nanowires of about 2 μm. The roots of the ZnO nanowires are electrically connected through a thick ZnO underlayer. Fig. 1(b) and (c) show typical SEM images of a dense array of ZnO–$ZnGa_2O_4$ core–shell nanowires under different magnifications. A homogeneous growth of the surrounding $ZnGa_2O_4$ shells on the ZnO nanowire cores was obtained over a large area. Moreover, the initial vertical alignment of the ZnO nanowires is well maintained in the ZnO–$ZnGa_2O_4$ core–shell nanowires. The average diameter of the ZnO–$ZnGa_2O_4$ core–shell nanowires is estimated to increase to about 90 nm from the original 60 nm. EDX analysis on the sidewall surface of one core–shell nanowire gave an atomic ratio of Zn/Ga/O of about 14/28/58 (~1/2/4), indicating the formation of the $ZnGa_2O_4$ phase. The tilted-angle SEM view of the same sample shown in Fig. 1(d) indicates that all the ZnO–$ZnGa_2O_4$ core–shell nanowires are well aligned, assembled in a high density and bonded together at their bases by a thick underlayer. Such densely packed core–shell nanowires realize an ideal structure for a photoanode to be used in photoelectrochemical water splitting.

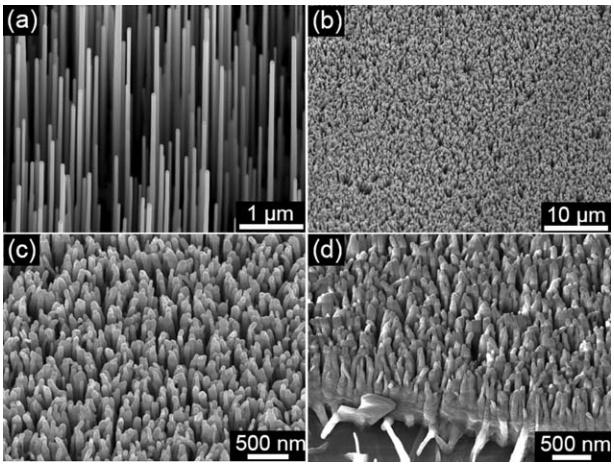

Fig. 1 SEM images of the ZnO and ZnO–$ZnGa_2O_4$ nanowire arrays. (a) Vertically aligned ZnO nanowires on the *a*-plane sapphire substrate. (b and c) The ZnO–$ZnGa_2O_4$ core–shell nanowire array on the *a*-plane sapphire substrate taken with different magnifications. (d) A cross-sectional image of the ZnO–$ZnGa_2O_4$ core–shell nanowire array.

XRD measurement was taken to characterize the ZnO nanowire array and the ZnO–$ZnGa_2O_4$ core–shell nanowire array. Fig. 2(a) shows typical XRD patterns of the nanowire samples. Only two sharp diffraction peaks indexed to the wurtzite ZnO (0002) and (0004) were observed with the ZnO nanowire array sample. This is strong evidence that the synthesized ZnO nanowires are well-aligned along the ZnO [0001] direction. Such highly oriented ZnO nanowires with single crystal quality, working as a growth template in the second CVD process, facilitate the synthesis of the ZnO–$ZnGa_2O_4$ core–shell nanowire array. The XRD pattern of ZnO–$ZnGa_2O_4$ nanowire array shows only four diffraction peaks indexed to the wurtzite ZnO (0002), (0004) and the spinel $ZnGa_2O_4$ (111), (222). This result is strong evidence for the formation of $ZnGa_2O_4$ shell layers well-aligned along the $ZnGa_2O_4$ [111] direction, as illustrated in the schematic of Fig. 2(c).

TEM and HRTEM analyses were further carried out to examine the crystal quality and crystallographic orientations of the ZnO core and the $ZnGa_2O_4$ shell. Fig. 2(b) shows a bright-field TEM image of a ZnO–$ZnGa_2O_4$ core–shell nanowire scratched

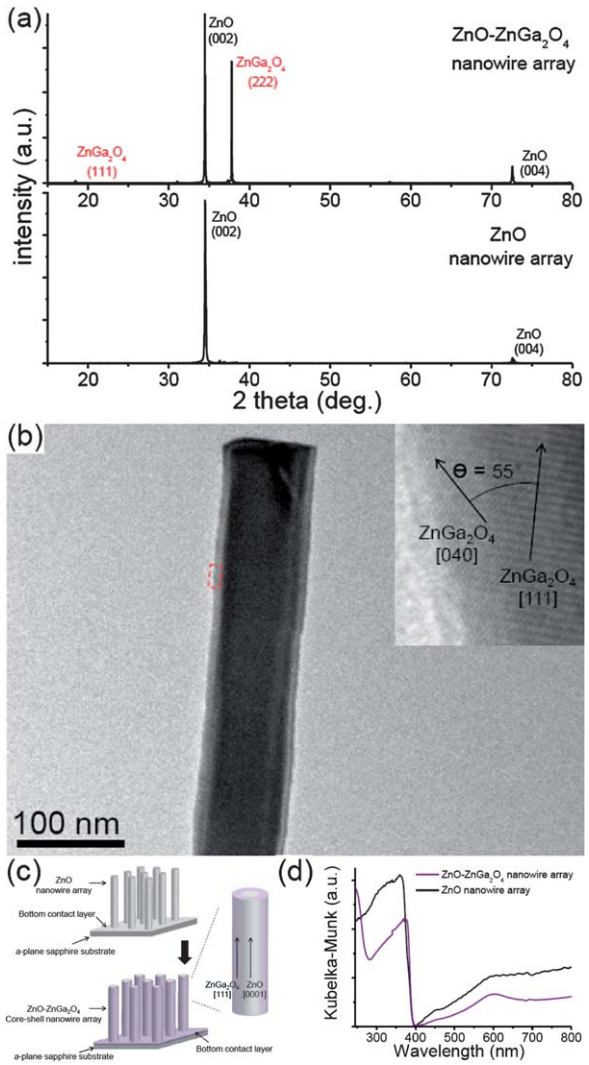

Fig. 2 (a) XRD patterns of the ZnO and ZnO–$ZnGa_2O_4$ nanowire arrays. (b) A bright-field TEM image of an individual ZnO–$ZnGa_2O_4$ core–shell nanowire. The inset is a HRTEM image of the $ZnGa_2O_4$ shell area (box area) of the core–shell nanowire. (c) A schematic of the ZnO–$ZnGa_2O_4$ core–shell nanowire array. (d) UV-VIS absorption spectra of the nanowire arrays for ZnO (black) and ZnO–$ZnGa_2O_4$ (purple).

from the ZnO–$ZnGa_2O_4$ nanowire array sample. The diameter of the nanowire core is about 65 nm, which is consistent with the average diameter of about 60 nm of the ZnO nanowires synthesized by the first-step CVD growth as observed with SEM. The overall diameter of the core–shell nanowire is about 85 nm from the TEM image, which is in agreement with the diameter of about 90 nm of the ZnO–$ZnGa_2O_4$ core–shell nanowires obtained with SEM observation. The HRTEM image of the shell region (inset) shows that the shell area of the nanowire consists of the single-crystalline spinel $ZnGa_2O_4$ phase. The calculated fringe spacing is 0.48 nm along the long axis direction of the core–shell nanowire, which is consistent with the value for the {111} plane spacing of the $ZnGa_2O_4$ spinel. Moreover, crystal fringes with a spacing of 0.21 nm were also observed on the shell area of the nanowire, which is consistent with the value of {040} plane spacing of the $ZnGa_2O_4$ spinel. The angle between these two planes is measured to be about 55° from the inset figure. It agrees with the angle value of 54.7° between [111] and [040] of the $ZnGa_2O_4$ spinel.[7] This result confirms the previous XRD analysis that [111] oriented $ZnGa_2O_4$ shells were formed on [0001] oriented ZnO nanowire cores, as shown in the schematic of Fig. 2(c). Parallel directions of the wurtzite ZnO [0001]//spinel $ZnGa_2O_4$ [111] and wurtzite ZnO [$\bar{2}$110]//spinel $ZnGa_2O_4$ [1$\bar{1}$0] are identified from our previous work.[8] Therefore, a hetero-epitaxial growth of the $ZnGa_2O_4$ shells on the ZnO nanowire cores takes place to form the ZnO–$ZnGa_2O_4$ core–shell nanowires.

Light absorption properties

Fig. 2(d) shows the UV-VIS absorption spectra of the ZnO nanowire array and ZnO–$ZnGa_2O_4$ core–shell nanowire array. In the absorption spectra of the ZnO nanowire array, one sharp absorption edge with an onset at 390 nm (corresponding to a band gap of 3.2 eV) is observed. This is attributed to the near-band-gap absorption of ZnO. In contrast, two clear absorption edges with onsets at 295 nm and 390 nm were observed in the absorption spectra of the ZnO–$ZnGa_2O_4$ core–shell nanowire array. The former absorption with the onset at 295 nm (corresponding to a band gap of 4.2 eV) is related to the near-band-gap absorption of the $ZnGa_2O_4$ shells.[8,9] The latter absorption has the same onset value of 390 nm to that of the ZnO nanowire array, and therefore is attributed to the near-band-gap absorption of the ZnO nanowire cores.

Electrochemical properties

To understand the electronic properties of the photoanode in electrolyte solution is of primary importance in the development of photoelectrochemical water splitting cells. Therefore, electrochemical impedance spectroscopy measurements were used to determine the carrier density of the nanowires and the flatband potential of the nanowires at nanowire/electrolyte interfaces. A solution of 0.5 M $NaClO_4$ was prepared for the electrolyte and buffered to a pH of 7.0 with a phosphate buffer solution. A three-electrode system was set in the electrolyte solution for the electrochemical impedance measurement. An Ag/AgCl electrode in saturated KCl solution was used as a reference electrode (+0.198 V *versus* NHE), a Pt wire was used as a counter electrode and the ZnO and ZnO–$ZnGa_2O_4$ nanowire arrays were used as working electrodes. In the preparation of working electrodes, indium was used to attach the copper wires onto the nanowire samples in order to form ohmic contacts. The contact areas between indium and nanowires were sealed by non-conductive and water-proof adhesive polymer layers. Prior to the electrochemical impedance analysis, N_2 gas was bubbled for 10 minutes to get rid of O_2 in the electrolyte solution. The cyclic voltammetry and Nyquist analysis were first measured in the dark to find out the suitable range of the applied bias and the frequency for the nanowire samples in the electrolyte solution. Then, Mott–Schottky analysis was performed with a bias varying from −1 V to 1 V (*versus* Ag/AgCl), at a frequency of 1 kHz, and under dark conditions. The measured Mott–Schottky data of the ZnO–$ZnGa_2O_4$ core–shell nanowire array together with the Mott–Schottky data of the ZnO nanowire array are plotted in Fig. 3(a). A more cathodic flatband potential of the ZnO–$ZnGa_2O_4$ nanowire array than the ZnO nanowire array can be observed from the curves in Fig. 3(a).

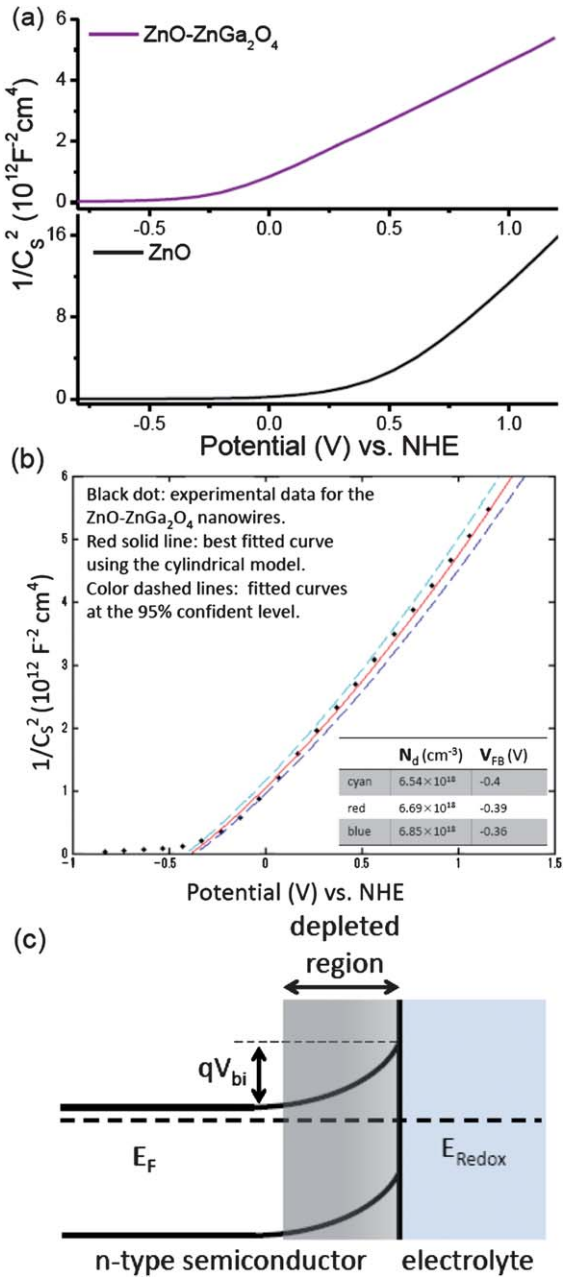

Fig. 3 (a) Mott–Schottky plots of the ZnO and ZnO–$ZnGa_2O_4$ nanowire arrays at a frequency of 1 kHz under dark conditions with a bias varying from −0.8 to 1.2 V (*versus* NHE). (b) Fitted curves in the Mott–Schottky plot of ZnO–$ZnGa_2O_4$ nanowire array with an assumed ε value of 10 for the ZnO–$ZnGa_2O_4$ nanowires. (c) A schematic of surface band bending at an idealized interface between an n-type semiconductor and an electrolyte in equilibrium. qV_{bi} is the energy barrier height at the interface.

The carrier density and flatband potential of a planar semiconductor at semiconductor/electrolyte interfaces can be calculated using the Mott–Schottky equations:[10]

$$N_d = \frac{2}{q\varepsilon\varepsilon_0\left[d\left(1/C_s^2\right)/dV\right]},$$

$$1/C_s^2 = 2(V - V_{FB})/q\varepsilon_0\varepsilon N_d,$$

where C_S is the capacitance per unit area of the semiconductor, V is the applied bias between the electrodes, V_{FB} is the flatband potential of the semiconductor at the semiconductor/electrolyte interface, q is the unit electron charge, ε_0 is the permittivity of vacuum and ε is the dielectric constant of the semiconductor.

However, a geometric effect of cylindrical semiconductor nanowires results in a deviation from the linear $1/C^2$ *vs.* V behaviour of a planar electrode Mott–Schottky plot. As Mora-Seró *et al.* reported,[11] the carrier density and flatband potential of the cylindrical nanowires can be quantified by solving the Poisson equation with a cylindrical capacitance approximation at the nanowire/electrolyte interfaces:

$$\frac{1}{r}\frac{\partial}{\partial r}\left(r\frac{\partial V}{\partial r}\right) = -\frac{q}{\varepsilon\varepsilon_0}N_d,$$

$$C_s = \frac{2\varepsilon\varepsilon_0 x^2}{R(R^2 - x^2)},$$

where R is the radius of the nanowires and x is the central radius of quasi-neutral region in the nanowires.[11] Therefore, the carrier density and flatband potential of the nanowires can be obtained by fitting the above equations to the experimental $1/C^2$ *vs.* V curves of the Mott–Schottky plots.

The carrier density of the ZnO–$ZnGa_2O_4$ nanowires was estimated to be 7×10^{18} cm^{-3} from the curves shown in Fig. 3(b). By the same method, the estimated carrier density of the ZnO nanowires was 2×10^{18} cm^{-3}. The increase in the carrier density of the ZnO–$ZnGa_2O_4$ nanowires compared to that of the ZnO nanowires is understood as the formation of conductive $ZnGa_2O_4$ shell layers[12] and the introduction of Ga donors in the ZnO cores.[8,13] The increase in the carrier density of the ZnO–$ZnGa_2O_4$ nanowires decreases the electrical resistance of the electrodes, thus leading to a reduced energy loss in photoelectrochemical water splitting.[6]

The flatband potential of the nanowires at the nanowire/electrolyte interfaces is another important parameter when analyzing photoanodes for photoelectrochemical water splitting. Band bending at the interfaces affects the recombination probability of the photo-generated electrons/holes and determines the required bias potential to apply for the electrolysis of water to occur. A clear understanding of the flatband potential and the surface band bending information of the anode material in the electrolyte solution is essential. Typically, a negative flatband potential and an upward band bending occur at the interface of an n-type semiconductor and an electrolyte, due to the Fermi-level difference between the n-type semiconductor and the electrolyte.[14] A schematic illustration of the band bending with a contact energy barrier at an idealized interface between an n-type semiconductor in equilibrium with an electrolyte is shown in Fig. 3(c). From the fitting results in Fig. 3(b), the flat-band potential V_{FB} of the ZnO–$ZnGa_2O_4$ core–shell nanowire array is estimated to be −0.4 V (*versus* NHE). The cathodic flatband potential of the ZnO–$ZnGa_2O_4$ core–shell nanowire array is attributed to the passivation of oxygen vacancies of the ZnO by the formation of $ZnGa_2O_4$ shells. In addition, $ZnGa_2O_4$ does not possess a strong surface adsorption property which might affect the surface band

bending of the semiconductor. More importantly, the enhanced cathodic flatband potential of the ZnO–$ZnGa_2O_4$ core–shell nanowire array compared to the ZnO nanowire array provides a more suitable energy band position for water splitting.[6]

Photoelectrochemical-water-splitting performance

Photocurrent properties of the ZnO and ZnO–$ZnGa_2O_4$ nanowire arrays when used as photoanodes were measured in a 0.1 M Na_2SO_4 electrolyte solution (at pH = 6) under illumination with a 300 W xenon lamp. An Ag/AgCl electrode in saturated KCl solution was used as a reference electrode and a Pt wire was used as a counter electrode. Fig. 4(a) shows the photoresponsive anode current of the ZnO–$ZnGa_2O_4$ nanowire array at a bias ranging from −0.8 V to 1 V (*versus* Ag/AgCl). Good photoresponsibility of the ZnO–$ZnGa_2O_4$ nanowire array is observed from the on/off light cycles in Fig. 4(a). The appearance of the anodic photocurrent indicates that the ZnO–$ZnGa_2O_4$ core–shell nanowire array functions as an n-type semiconductor. This agrees with the previous result of positive slope (positive value of $d(1/C_S^2)/dV$) in the Mott–Schottky plot of the ZnO–$ZnGa_2O_4$ nanowire array, which also indicates an n-type semiconductor property of the ZnO–$ZnGa_2O_4$ core–shell nanowires. Moreover, the anodic photocurrent appeared at −0.55 V *vs.* Ag/AgCl (−0.35 V *vs.* NHE), as indicated in the inset of Fig. 4(a). The flatband potential V_{FB} of the ZnO–$ZnGa_2O_4$ core–shell nanowires is equivalent to the onset potential of anodic photocurrent.[15] Thus, the V_{FB} of the ZnO–$ZnGa_2O_4$ nanowire array was estimated to be -0.35 ± 0.1 V (*vs.* NHE), which is in agreement with our previous calculated value of −0.4 V obtained from the Mott–Schottky plot.

An amperometric study of the ZnO–$ZnGa_2O_4$ core–shell nanowire array was performed at a fixed bias of 0.7 V *versus* Ag/AgCl with on–off illumination cycles. The obtained data are plotted in the form of a current–time curve in Fig. 4(b). The result shows a very low current of $<10^{-4}$ mA cm^{-2} in the dark conditions. It indicates that no chemical reaction of electrolysis occurred with the anode of the ZnO–$ZnGa_2O_4$ core–shell nanowire array at the applied bias of 0.7 V under dark conditions. Upon illumination, a spike value of photocurrent is observed first due to the transient effect in power excitation[1] and then the photocurrent quickly returned to a steady value of 1.2 mA cm^{-2}, indicating a stable photoelectrolysis reaction occurred at the anode of ZnO–$ZnGa_2O_4$ core–shell nanowire array. After switching off the light, a fast recovery of the current to the dark current value is clearly observed. The on/off light cycles of the current show good reproducibility and anti-photocorrosion stability from the current–time curve. In contrast, a very unstable photocurrent with the ZnO nanowire array was observed at a fixed bias of 0.7 V *versus* Ag/AgCl as shown in Fig. 4(c). The unstable photocurrent with the anode of ZnO nanowire array originates from the photodecomposition of ZnO nanowires in the electrolyte solution. As a result, the formation of the $ZnGa_2O_4$ shells on the ZnO nanowires passivates the strong surface adsorption effect of the ZnO nanowires, resulting in a more favorable band edge position for the oxidation of water in photoelectrochemical water splitting. Moreover, the formation of the $ZnGa_2O_4$ shells enhances the carrier density of the nanowires, leading to an increased electron transfer in the photoanode and therefore a reduced energy loss in photoelectrochemical water splitting. The chemical stability of the nanowire array is also improved by the formation of the $ZnGa_2O_4$ shells. Therefore, the synthesized ZnO–$ZnGa_2O_4$ core–shell nanowire array provides enhanced stability and electronic properties for the use in the photoelectrochemical water splitting applications.

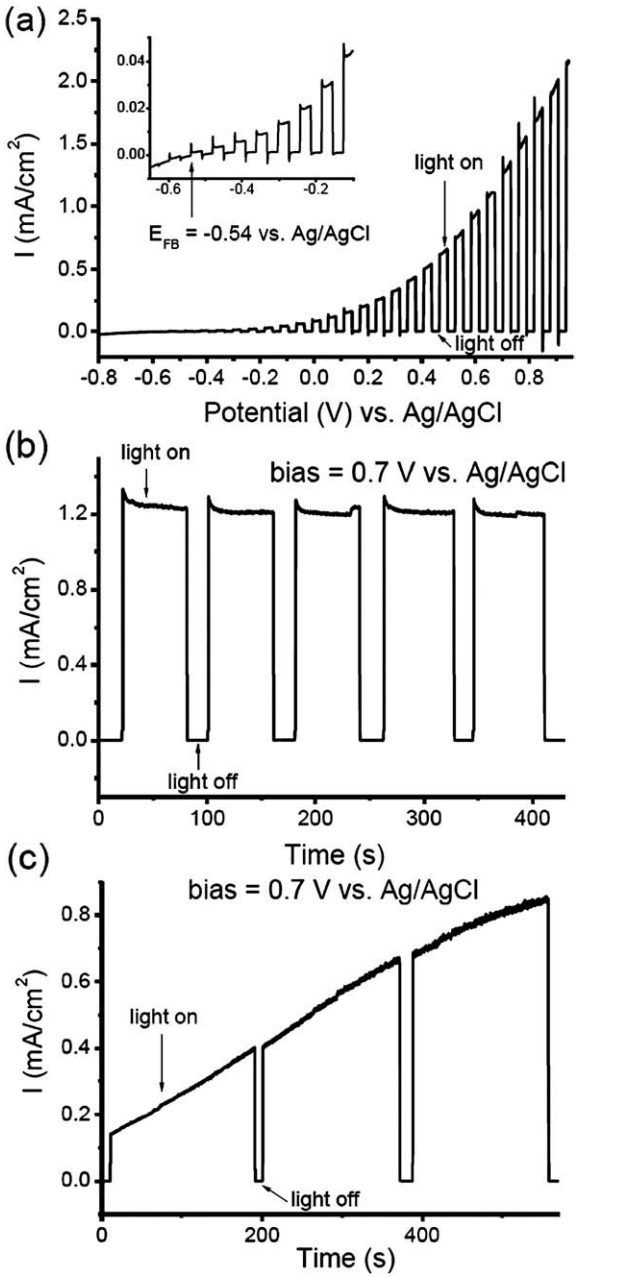

Fig. 4 (a) Current–voltage curves of the ZnO–$ZnGa_2O_4$ nanowire array in an electrolyte of 0.1 M Na_2SO_4 (at pH = 6) under illumination with a 300 W xenon lamp. Sweep rate of the voltage was 0.5 mV s^{-1}. (b) A current–time curve of the ZnO–$ZnGa_2O_4$ nanowire array when used as an anode at an applied bias of 0.7 V (*versus* Ag/AgCl) with light on (for 60 s) and off (for 20 s) over 5 cycles. (c) A current–time curve of the ZnO nanowire array at an applied bias of 0.7 V (*versus* Ag/AgCl) with light on (for 180 s) and off (for 15 s) over 3 cycles.

Conclusions

A dense array of vertically aligned ZnO–$ZnGa_2O_4$ core–shell nanowires was synthesized in large scale on the *a*-plane sapphire substrate by a simple two-step CVD method. The ZnO cores and $ZnGa_2O_4$ shells of the nanowires are of single crystal quality and have aligned crystallographic orientations as evidenced from XRD and TEM analyses. The electronic property and the photocurrent performance of the ZnO and ZnO–$ZnGa_2O_4$ nanowire arrays were investigated in detail. Mott–Schottky analysis and photoresponsive current–voltage measurement both confirm an n-type semiconductor property, a flat-band potential of −0.4 V (*versus* NHE) and a carrier density of 7×10^{18} cm^{-3} for the ZnO–$ZnGa_2O_4$ nanowire array. Compared to the ZnO nanowire array, a more favorable energy band position for the photo-electrolysis of water and an increased carrier density for the electron transfer were obtained with the ZnO–$ZnGa_2O_4$ core–shell nanowire array. Photocurrent measurement with the ZnO–$ZnGa_2O_4$ core–shell nanowires at an applied bias of +0.7 V (*versus* Ag/AgCl) gives a stable and large photocurrent of 1.2 mA cm^{-2} under a 300 W xenon lamp illumination. Moreover, a very low current of $<10^{-4}$ mA cm^{-2} was obtained with the ZnO–$ZnGa_2O_4$ core–shell nanowires at +0.7 V bias (*versus* Ag/AgCl) under dark conditions. The fabricated dense ZnO–$ZnGa_2O_4$ core–shell nanowire array provides stable anti-photocorrosion ability and enhanced electronic properties for use as a photo-anode in photoelectrochemical water splitting.

Acknowledgements

This work was supported through the JSPS program, "Japan Society for the Promotion of Science," Global COE Program, "Global Center of Excellence for Mechanical Systems Innovation," and Grants-in-Aid for Scientific Research (B) 22360056 from the Ministry of Education, Culture, Sports, Science and Technology (MEXT), Japan. The authors thank Prof. Kazunari Domen and Prof. Jun Kubota (Department of Chemical System Engineering, The University of Tokyo) for the UV-VIS diffuse reflectance spectra and photocurrent measurements.

References

1 X. Yang, A. Wolcott, G. Wang, A. Sobo, R. C. Fitzmorris, F. Qian, J. Z. Zhang and Y. Li, *Nano Lett.*, 2009, **9**, 2331–2336.
2 R. V. D. Krol, Y. Liang and J. Schoonman, *J. Mater. Chem.*, 2008, **18**, 2311–2320.
3 Y. J. Huang, A. Boukai and P. D. Yang, *Nano Lett.*, 2009, **9**, 410–415.
4 H. J. Fan, Y. Yang and M. J. Zacharias, *J. Mater. Chem.*, 2009, **19**, 885–900.
5 D. Deng, S. T. Martin and S. Ramanathan, *Nanoscale*, 2010, **2**, 2685–2691.
6 T. Bak, J. Nowotny, M. Rekas and C. C. Sorrell, *Int. J. Hydrogen Energy*, 2002, **27**, 991–1022.
7 K. Chang and J. Wu, *J. Phys. Chem. B*, 2005, **109**, 13572–13577.
8 M. Zhong, Y. Li, T. Tokizono, M. Zheng, Y. Yamada and J. J. Delaunay, *J. Nanopart. Res.*, submitted.
9 N. Kumagai, L. Ni and H. Irie, *Chem. Commun.*, 2011, **47**, 1884–1886.
10 S. M. Sze and K. K. Ng, *Physics of Semiconductor Devices*, John Wiley & Sons, Inc, 3rd edn, 2007.
11 I. Mora-Seró, F. Fabregat-Santiago, B. Denier and J. Bisquert, *Appl. Phys. Lett.*, 2006, **89**, 203117.
12 T. Omata, N. Ueda and K. Ueda, *Appl. Phys. Lett.*, 1994, **64**, 1077–1078.
13 G. Yuan, W. Zhang, J. Jie, X. Fan, J. Tang, I. Shafiq, Z. Ye, C. Lee and S. Lee, *Adv. Mater.*, 2008, **20**, 168–173.
14 S. R. Morrison, *Electrochemistry at Semiconductor and Oxidized Metal Electrodes*, Plenum, New York, 1980.
15 H. Hashiguchi, K. Meada, R. Abe, A. Ishikawa, J. Kubota and K. Domen, *Bull. Chem. Soc. Jpn.*, 2009, **82**, 401–407.

